Original Article

MOLECULAR METABOLISM

Improvement of MASLD and MASH by suppression of hepatic N-acetyltransferase 10

Yanying Yang[1,2,3,8], Jie Lu[4,8], Yuejun Liu[5,8], Ni Zhang[6], Yunchen Luo[7], Mingyue Ma[1,4], Zhixia Dong[1], Shuo Zhang[1], Ming-Hua Zheng[6], Cheng-Chao Ruan[2], Xinjian Wan[1], Cheng Hu[4], Yan Lu[1,*], Xiaojing Ma[4,], Bing Zhou[1,4,***]**

ABSTRACT

Objective: Metabolic dysfunction-associated steatotic liver disease (MASLD) and metabolic dysfunction-associated steatohepatitis (MASH) are characterized by excessive triglyceride accumulation in the liver. However, due to an incomplete understanding of its pathogenesis, more efforts are needed to identify specific and effective treatments. N4-acetylcytidine (ac4C) is a newly discovered RNA modification to regulate mRNA. N-acetyltransferase 10 (NAT10) has not been fully explored in MASLD and MASH.

Methods: The clinical relevance of NAT10 was evaluated based on its expression in various mouse and human models of MASLD and MASH. Acetylated RNA immunoprecipitation sequencing and mRNA stability assays were used to explore the role of NAT10 in regulating ac4C modification and expression of target genes. Genetically engineered mice were employed to investigate the role of NAT10 in MASLD and MASH progression.

Results: Hepatic NAT10 expression was significantly increased in multiple mice and humans of MASLD and MASH. Genetic knockout of NAT10 protected mice from diet-induced hepatic steatosis and steatohepatitis, whereas overexpression of NAT10 exacerbated high-fat-diet-induced liver steatosis. Mechanistically, NAT10 binds to *Srebp-1c* mRNA, promoting its stability and expression, thereby upregulating lipogenic enzymes. Treatment with Remodelin, a NAT10-specific inhibitor, effectively ameliorates liver steatosis and dyslipidemia in a preclinical mouse model.

Conclusions: Our findings indicate that NAT10 could regulate lipid metabolism in MASLD and MASH by stabilizing *Srebp-1c* mRNA and upregulating lipogenic enzymes. This study highlights the role of NAT10 and RNA acetylation in the pathogenesis of MASLD and MASH. Thus, our findings suggest a promising new therapeutic approach, such as the use of NAT10 inhibitor, for treating metabolic liver disease.

Keywords Metabolic dysfunction-associated steatotic liver disease; Metabolic dysfunction-associated steatohepatitis; N4-acetylcytidine; N-acetyltransferase 10

1. INTRODUCTION

Metabolic dysfunction-associated steatotic liver disease (MASLD), originally known as non-alcoholic fatty liver disease (NAFLD), has become the most common chronic liver disease worldwide due to its high prevalence [1,2]. MASLD includes simple steatosis and metabolic dysfunction-associated steatohepatitis (MASH), which can further progress into liver fibrosis, cirrhosis and hepatocellular carcinoma [1,2]. Global epidemiology of liver cancer from 2010 to 2019 showed that MASH is the fastest growing cause of liver cancer [3,4]. Therefore, insights into the pathogenesis of MASLD and MASH are of crucial importance for identifying new therapeutic targets.

[1]Institute of Metabolism and Regenerative Medicine, Digestive Endoscopic Center, Shanghai Sixth People's Hospital Affiliated to Shanghai Jiao Tong University School of Medicine, Shanghai, China [2]Department of Physiology and Pathophysiology, Shanghai Key Laboratory of Bioactive Small Molecules, State Key Laboratory of Medical Neurobiology, School of Basic Medical Sciences, and Jinshan Hospital, Fudan University, Shanghai, China [3]Department of Endocrinology, Zhongnan Hospital of Wuhan University, Wuhan, China [4]Shanghai Diabetes Institute, Department of Endocrinology and Metabolism, Shanghai Key Laboratory of Diabetes Mellitus, Shanghai Clinical Centre for Diabetes, Shanghai Sixth People's Hospital Affiliated to Shanghai Jiao Tong University School of Medicine, Shanghai, China [5]Department of Endocrinology and Metabolism, Zhongshan Hospital, Fudan University, Shanghai, China [6]MAFLD Research Center, Department of Hepatology, The First Affiliated Hospital of Wenzhou Medical University, Wenzhou, Zhejiang, China [7]Department of Endocrinology and Metabolism, Shanghai General Hospital Affiliated to Shanghai Jiao Tong University, Shanghai, China

[8] Yanying Yang, Jie Lu and Yuejun Liu contributed equally to this work.

*Corresponding author. E-mail: luyan5011@shsmu.edu.cn (Y. Lu).

**Corresponding author. E-mail: maxiaojing@sjtu.edu.cn (X. Ma).

***Corresponding author. E-mail: zhoubing2023@126.com (B. Zhou).

Abbreviations: MASLD, metabolic dysfunction-associated steatotic liver disease; MASH, metabolic dysfunction-associated steatohepatitis; ac4C, N4-acetylcytidine; NAT10, N-acetyltransferase 10; TG, triglyceride; DNL, *de novo* lipogenesis; SREBP-1c, sterol regulatory element-binding protein 1c; FASN, fatty acid synthase; SCD1, stearoyl-CoA desaturase 1; ACC1, acetyl-CoA carboxylase 1; TC, total cholesterol; ALT, alanine transaminase; AST, aspartate transaminase

Received June 14, 2024 • Revision received August 13, 2024 • Accepted September 11, 2024 • Available online 16 September 2024

https://doi.org/10.1016/j.molmet.2024.102030

MASLD and MASH are mainly attributed to the disturbance in hepatic triglyceride (TG) homeostasis, that is, an overabundance of *de novo* lipogenesis (DNL) or uptake of fatty acids, exceeding the capacity for fatty acid oxidation and very-low-density lipoprotein secretion [5,6]. DNL is a multifaceted metabolic process converting acetyl-CoA into TG through multiple chemical reactions. At the molecular level, the rate of DNL is controlled by sterol regulatory element-binding protein 1c (SREBP-1c), a master transcription factor upregulating most of rate-limiting enzymes for DNL, including fatty acid synthase (FASN), stearoyl-CoA desaturase 1 (SCD1) and acetyl-CoA carboxylase 1 (ACC1) [7–9]. The role of increased lipogenesis in liver steatosis has been well acknowledged by decades of studies [10]. Notably, expression levels of SREBP-1c are significantly increased in the livers from patients with MASLD and MASLD mouse models [10]. At the transcription level, *Srebp-1c* mRNA expression is upregulated by several transcription factors, such as the nuclear receptor LXRα [11]. Our previous studies also identified some new transcription factors that transcriptionally regulate SREBP-1c expression, including Sox4, YY1-FXR-SHP axis and FOXA3-Per1 axis [12–14]. In addition, at the protein level, SREBP-1c protein is stabilized by HDAC1 through the desuccinylation, which contributes to the pathogenesis of hepatic steatosis under endotoxin challenge or inflammatory status [15]. Moreover, recent studies including ourselves demonstrated that RNA modification is also an important mechanism for regulating SREBP-1c expression and MASLD. For instance, we found that YTHDC2, a reader protein of N6-methyladenosine (m6A) modification, could bind to *Srebp-1c* mRNA to decrease its stability, thereby inhibiting its expression [16]. YTHDC2 is downregulated in patients with MASLD and MASLD mice, contributing to the upregulation of SREBP-1c and lipogenic enzymes [16].

N4-acetylcytidine (ac4C) acetylation is a newly identified modification in eukaryotic mRNAs [17], but its biological significance remains largely unexplored. Until now, N-acetyltransferase 10 (NAT10) serves as the sole key catalytic enzyme involved in mRNA acetylation. Recent studies showed that NAT10 expression and RNA ac4C levels were elevated in cardiac remodeling models and patients with cardiac hypertrophy [18]. NAT10 inhibition could attenuate Ang II-induced cardiomyocyte hypertrophy and cardio fibroblast activation [18]. Besides, NAT10-mediated ac4C acetylation of *Tfec* mRNA promotes cardiomyocyte apoptosis following myocardial infarction [19]. Additionally, NAT10 was shown to acetylate and stabilize *Col5a1* mRNA, thereby promoting epithelial-to-mesenchymal transition and metastasis [20]. These findings collectively underscore the roles of NAT10 in cardiovascular diseases and tumorigenesis. However, the roles of ac4C acetylation and NAT10 in other human diseases, especially in the regulation of MASLD and MASH pathogenesis, remains poorly understood.

In the present study, we demonstrate that ac4C RNA modification and NAT10 is involved in the regulation of hepatic lipid metabolism. Our results showed that NAT10-mediated acetylation of *Srebp-1c* mRNA promotes its mRNA stability and expression, contributing to MASLD and MASH. Pharmacological suppression of NAT10 by Remodelin could improve liver steatosis and dyslipidemia in a preclinical mouse model of MASLD.

2. MATERIALS AND METHODS

2.1. Animal experiments

8-week-old C57BL/6 male mice were obtained from Shanghai Lingchang Biotechnology Co., Ltd. (Shanghai, China). NAT10 flox/flox mice (Strain No. T007971) mice, Albumin-Cre mice (Strain No. T003814), *db/db* mice (Strain No. T002407) and *ob/ob* mice (Strain No. T001461) were obtained from Gempharmatech Co., Ltd (Nanjing, China). Liver-specific NAT10 knockout mice were generated by crossing NAT10 flox/flox mice with Albumin-Cre mice. High-fat diets (HFD) containing 60% kcal from fat, 20% kcal from carbohydrates, and 20% kcal from protein were purchased from Research Diets (Catalog D12492, New Brunswick, New Jersey, USA). MASH mice model was established by HFHC diets (also called GAN diets, 40% kcal fat, 20% kcal fructose, and 2% cholesterol; Catalog D09100310, Research Diets). To pharmacologically suppress NAT10 *in vivo*, mice were treated with daily intraperitoneal injection of Remodelin (20 mg/kg, Catalog S7641, Selleck, China) or vehicle control for 16 days. The animal experiments were reviewed and approved by the Animal Care Committees of Shanghai Jiao Tong University School of Medicine.

2.2. Human samples

All participants underwent physical examinations, blood biochemical tests, and ultrasound assessments at Zhongshan Hospital, Fudan University. Normal liver tissues were obtained during gallbladder exclusion excision surgery performed for gallbladder stones. Diagnosis of MASLD was based on the presence of $\geq$5% hepatic steatosis. Exclusion criteria encompassed known acute or chronic viral hepatitis, excessive alcohol consumption, use of pharmacological treatments (hepatic protectants or hepatotoxic agents), chronic kidney disease, severe cardiovascular or cerebrovascular disease, significant gastrointestinal disorders or gastrointestinal surgery, and history of malignant tumors. Written informed consent was obtained from each participant. The human study was approved by the Human Research Ethics Committee of Zhongshan Hospital and conducted in accordance with the 1975 Declaration of Helsinki.

2.3. Adenovirus and adeno-associated virus

Recombinant adenovirus (Ad-) used for liver-specific overexpression of NAT10, was constructed by cloning the full-length mouse *Nat10* cDNA into GV176 adenoviral vector (CMV-MCS) (GeneChem, Shanghai, China). To knockout NAT10 in the livers of adult mice, NAT10 flox/flox mice were administered with adenovirus containing Cre recombinase. Adenovirus containing GFP (Ad-GFP) was used as negative controls. Mice were administered 1×10^9 pfu of purified Ad or 1×10^{11} pfu of purified AAV, respectively. All viruses were purified by cesium chloride, dialyzed in PBS containing 10% glycerol and administered to mice via tail vein injection.

2.4. Liver triglyceride contents

Liver triglyceride contents were measured using commercial kits purchased from Applygen company (Catalog E1025, Beijing, China) according to the manufacturer's instructions. Briefly, 50 mg of mouse liver tissues were placed into the lysis solution and thoroughly grounded. The homogenates were subsequently heated in a 70 °C water bath for 10 min and centrifuged at 2000 rpm for 5 min. Supernatants were collected and measured by spectrophotometer.

2.5. Plasma biochemical measurements

After anesthesia, blood was collected from mice posterior orbital venous plexus into anticoagulant tubes, and centrifuged at 3000 rpm for 15 min to assemble the supernatant. Plasma triglyceride (TG), total cholesterol (TC), alanine transaminase (ALT), and aspartate transaminase (AST) levels were measured using commercial kits following the manufacturer's instructions (Kehua, Shanghai, China).

2.6. Histology analysis, F4/80 staining, and Sirius red staining

The liver tissues were placed in 10% neutral-buffered formalin (Catalog G1101, Servicebio, Wuhan, China), embedded in paraffin, and cut

into 5 μm sections for staining. Liver fibrosis was evaluated by Sirius red staining as well as Masson's trichrome staining. For Oil Red O staining, frozen sectioned liver tissues were stained with Oil Red O according to standard procedures. For F4/80 immunohistochemical staining, the sections were incubated with 3% H_2O_2 at room temperature for 30 min to quench the endogenous peroxidase activity and then blocked in 3% BSA for 1 h. Tissues were cultivated with anti-F4/80 antibody (1:1000, Catalog GB11027, Servicebio, Wuhan, China) and Ly6g staining (1:1000, Catalog GB11229, Servicebio, Wuhan, China) overnight at 4°C and then incubated with an HRP-conjugated secondary antibody (1:200, Catalog GB1213, Servicebio). Images were assessed and quantitated by ImageJ software.

2.7. RNA isolation and quantitative real-time PCR

Total RNA was isolated from mouse liver tissues and cell lysates using commercial kits from Promega (Catalog LS1040, Beijing, China). First-strand cDNA was synthesized from total RNA using the Reverse Transcription System (Catalog RR036A, Takara Biotechnology, Japan). Oligo dT was used to prime cDNA synthesis. To analyze expression levels of target genes, quantitative real-time PCR (qRT-PCR) was performed by SYBR Green Premix Ex Taq (Catalog RR820A, Takara Biotechnology, Japan) on LightCycler 480 (Roche, Basel, Switzerland). Relative quantification analysis of gene expression was performed based on the $2^{-\Delta\Delta}$Ct method and normalized to the expression level of housekeeping gene *Rplp0*. The primer sequences for real-time qPCR are listed in Supplementary Table S1.

2.8. Protein extraction and Western blot

Mouse liver proteins were extracted using RIPA lysis buffer, and protein concentrations were quantified using commercial kits (Catalog A53225, ThermoFisher, USA). All protein samples were equally subjected to 10% SDS polyacrylamide gels, transferred to polyvinylidene difluoride membranes by electrophoresis, incubated with primary and secondary antibodies, and finally visualized by a chemiluminescence detection kit (Catalog WBKLS0500, Millipore, USA). The following primary antibodies were used: anti-GAPDH antibody (1:5000, Catalog 60004-1-Ig, Proteintech, China), anti-β-Actin (1:2000, Catalog 66009-1-Ig, Proteintech, China), anti-NAT10 antibody (1:2000, Catalog ab194297, Abcam, UK), anti-SREBP1 antibody (1:2000, Catalog sc-365513, Santa Cruz, USA), anti-α-Tubulin (1:2000, Catalog 11224-1-AP, Proteintech, China). Quantitation of immunoblots was assessed by Image J software.

2.9. RNA-sequencing and acRIP-Sequencing

acRIP-seq and RNA-seq analysis (CloudSeq Inc., Shanghai, China) were performed on liver tissues from four *db/db* mice and four lean mice, respectively. Total RNAs were depleted with rRNA by Ribo-zero (Illumina) and then subjected to immunoprecipitation with the GenSeqTM ac4C-IP Kit (GenSeq Inc., China) following the manufacturer's instructions. Briefly, RNAs were randomly fragmented to ~200 nt by RNA Fragmentation Reagents. Protein A/G beads were coupled to the ac4C antibody by rotating at room temperature for 1 h. The RNA fragments were incubated with the bead-linked antibodies and rotated at 4 °C for 4 h. The RNA/antibody complexes were then digested with Proteinase K and the eluted RNAs were purified by phenol: chloroform extraction. RNA libraries for immunoprecipitation and input samples were then constructed with NEBNext® Ultra II Directional RNA Library Prep Kits (New England Biolabs, Inc., USA) by following the manufacturer's instructions. Libraries were qualified using Agilent 2100 bioanalyzer and then sequenced in a HiSeq platform (Illumina). Paired-end reads were harvested from Illumina HiSeq 4000 sequencer and were quality controlled by Q30. After 3′ adaptor-trimming and low-quality reads removed by cutadapt software (v1.9.3). First, clean reads of all libraries were aligned to the reference genome (MM10) by Hisat2 software (v2.0.4). Acetylated sites on RNAs (peaks) were identified by MACS software. Differentially acetylated sites were identified by diffReps. These peaks identified by both software overlapping with exons of mRNA were figured out and chosen by home-made scripts. Subsequently, proprietary program was used to select sites that overlap with the exons of protein-coding genes. The stringent default screening criteria included a P-value threshold of $\leq$0.0001 and a minimum Fold Change of $\geq$2. We conducted a Gene Ontology (GO) functional analysis to explore the potential functions of mRNAs identified as differentially enriched. This analysis categorized the genes based on their biological processes, molecular functions, and cellular components. Astringent threshold of P value less than 0.05 was used to determine statistical significance, ensuring that the inferred functions are robust and reliable. Visualization of DMMS alignment was performed through the Integrative Genomics Viewer (IGV, http://www.broadinstitute.org/igv/) according to the manufacturer's instructions.

2.10. RNA immunoprecipitation

RNA Immunoprecipitation (RIP) experiments were performed using Magna RIP RNA-Binding Protein Immunoprecipitation Kits (Catalog 17-700, Millipore, Bedford, MA, USA) according to the manufacturer's instructions. Briefly, harvested Hepa1-6 cells were lysed with RIP lysis buffer on ice and then incubated with anti-NAT10 antibody (Catalog ab194297, Abcam, UK), anti-ac4C antibody (Catalog ab252215, Abcam, UK) or IgG antibody (Catalog 637712, Millipore, Bedford, MA, USA) overnight at 4 °C. Immunoprecipitated RNAs were isolated by TRIzol reagents (Invitrogen, CA, USA) and analyzed by qRT-PCR. The primer sequences of *Srebp-1c* were as following: Forword:5′-CTGGTGAGTGGAGGGACCAT-3′, Reverse:5′-GACCGGTAGCGCTTC TCAAT- 3′.

2.11. mRNA lifetime

Srebp-1c mRNA stability was determined in Hepa1-6 cells transfected with Ad-NAT10 or Ad-GFP for 12 h and WT/LKO mouse primary hepatocyte in the presence of actinomycin D (5 μg/ml) (Catalog A9415, Sigma—Aldrich, Saint Louis, USA) for 6 h, 3 h and 0 h, respectively. Then, total RNAs were isolated by TRIzol and expression levels of transcripts of interest were detected by qRT-PCR. With the treatment of actinomycin D, the mRNA transcription was turned off and the degradation rate of mRNA (Kdecay) was estimated by the following equation: $\ln(C/C_0) = -K_{decay}t$, in which t is transcription inhibition time (h), while C and C0 represent mRNA quantity at time t and time 0. The degradation of *Srebp-1c* mRNA followed a first order kinetics and the half-life was calculated by $t1/2 = \ln 2/K_{decay}$, whereas the K_{decay} values were extracted from the exponential trendlines (line of best fit).

2.12. Mouse primary hepatocytes

Mouse primary hepatocytes were isolated from 8- to 10-week-old mice using a collagenase buffer. Liver tissues were homogenized and filtered to create a cell suspension, and then centrifuged to separate the supernatant from the cell pellet. The pellet enriched with primary hepatocytes was mixed with a Percoll purification solution and centrifuged at 700 g for 10 min to eliminate cellular debris. The supernatant was subjected to repeated centrifugation at 500 g for 5 min to harvest non-parenchymal cells (NPCs). The freshly isolated hepatocytes were resuspended in DMEM supplemented with 10% FBS, 100 U/ml penicillin, and 100 μg/ml streptomycin (1% Pen-Strep), and plated at a density of 0.4×10^6 cells per well in a 6-well plate. 24 h

later, hepatocytes were treated with palmitic acid (200 μM) and infected with adenovirus or transfected with either siRNA targeting Srebp-1c or a negative control siRNA (NC).

2.13. siRNA transfection

For knockdown experiments in hepatocytes, cells were transfected with Ad-GFP plus negative control siRNA, Ad-NAT10 plus negative control siRNA, or Ad-NAT10 plus siRNA targeting Srebp-1c using a transfection reagent (Lipo3000, Invitrogen, CA, USA). The sequences of siRNAs were: negative control: 5′-UCUCCGAACGUGUCACGUTT-3′; Srebp-1c: 5′-GCGGCUGUU GUCUACCAUATT-3′.

2.14. Measurement of liver hydroxyproline contents

Hydroxyproline levels were determined utilizing a commercial assay kit (K226-100, Biovision). Liver tissues were homogenized in distilled water and subjected to hydrolysis with 10 N NaOH at 120 °C for 1 h. Following hydrolysis, 10 N HCl was added to neutralize the remaining NaOH. The mixture was then centrifuged at 10,000 g for 5 min to separate the supernatant. The supernatant was analyzed for absorbance at 560 nm using a microplate reader, following the manufacturer's protocol. The hydroxyproline contents were calculated from the absorbance values and normalized to the total protein contents.

2.15. Statistics

Data are presented as mean ± SEM. All statistical analysis was performed with GraphPad Prism Software (version 10, GraphPad, USA). Statistical differences between two groups were analyzed using the two-tailed unpaired t-test. One way ANOVA was used to compare more than two groups containing one factor. Pearson correlation analysis was used to analyze the correlation between gene expression levels and clinical parameters. A significance threshold of $P < 0.05$ was adopted. Statistical significance is displayed as $^{*}P < 0.05$, $^{**}P < 0.01$, or $^{***}P < 0.001$.

3. RESULTS

3.1. ac4C RNA modification is increased in the livers of MASLD mice

To explore whether ac4C RNA modification was involved in the MASLD pathogenesis, we performed acRIP-Seq together with RNA-Seq using mRNA samples from the livers of *lean* and leptin receptor-deficient (*db/db*) mice. AcRIP-Seq revealed that ac4C acetylation was elevated in *db/db* mice in CDS (58.43% vs. 61.32%), stop codon (10.92% vs. 10.52%), and 5′-UTR (7.53% vs. 6.77%) and 3′-UTR (2.99% vs. 3.34%) (Supplementary Figure 1A). acRIP-Seq identified a substantial amount of acetylation peaks, characterized by the typical 'CXXCXXCXX' motif [17], enriched in the vicinity of the CDS in mRNAs (Supplementary Figure 1A and B). Further analysis revealed distinct acetylation patterns with 9262 ac4C peaks (1857 protein-coding transcripts) in *db/db* mice and 6679 ac4C peaks (1265 protein-coding transcripts) in *lean* mice unique to each group, which covered 9568 ac4C peaks (5479 protein-coding transcripts) (Supplementary Figure 1C). Through intersection analysis of acRIP-Seq and RNA-Seq, we found that 466 genes were overlapped and significantly differentially expressed at both mRNA levels and ac4C modification levels. Interestingly, mRNA levels and ac4C modification levels of 275 genes were upregulated, suggesting that these genes might be targets of ac4C modification (Supplementary Figure 1D). Gene ontology (GO) analysis further found that these genes are enriched in the lipid metabolic process and lipid biosynthesis (Supplementary Figure 1E). Utilizing the Integrative Genomics Viewer (IGV) software, we investigated the acetylation patterns of lipid metabolism-associated genes. We observed a substantial increase in the acetylation levels of several genes involved in lipogenesis, including *Srebf1* (encoding SREBP-1c), *Fasn, Scd1, Acc1* (Supplementary Figure 1F—I). Together, these results suggest that ac4C mRNA modifications are involved in the regulation of hepatic lipid metabolism. This regulation might be responsible for the abnormal expression of lipogenic genes in the livers of MASLD mice.

3.2. NAT10 expression is elevated in MASLD and MASH mice

Our sequencing data suggested a potential role of altered ac4C mRNA acetylation patterns in predisposing hepatocytes to enhanced lipogenesis and, eventually, steatosis.

We firstly evaluated the expression and cellular localization of NAT10, the sole enzyme responsible for ac4C mRNA acetylation, in the liver. Western Blots showed that NAT10 is mainly expressed in hepatocytes (Supplementary Figure 2A). We also examined NAT10 expression in human livers using public scRNA-seq dataset (GSE158723), which showed that NAT10 expression is primarily expressed in hepatocytes (Supplementary Figure 2B). Then, we examined the expression level of NAT10 in *db/db* mice, *ob/ob* mice and HFD diet-fed C57BL/6 mice, which were widely used as mouse models of MASLD [21—24]. The liver samples of these mice have been used in our previous studies [16,25]. Quantitative real-time PCR (qRT-PCR) and western blots found that mRNA and protein levels of NAT10 were elevated in the livers of *db/db* mice, *ob/ob* mice and high-fat diet (HFD) fed mice, compared with their corresponding control mice (Figure 1A—F). Besides, previous studies including ourselves showed that long-term consumption of **h**igh-**f**at diet containing **h**igh **c**holesterol and high fructose (HFHC), also known as GAN diet, could induce MASH in mice, which mimics the pathology of patients with MASH [24—26]. As a result, expression levels of NAT10 were significantly upregulated in the livers of HFHC diet-induced MASH mice (Figure 1G and H). Collectively, multiple mouse models highlight that the upregulation of NAT10 is a conserved feature in MASLD and MASH.

3.3. NAT10 expression is increased in patients with MASLD

We next examined NAT10 expression in patients with MASLD. mRNA expression levels of *Nat10* and *Srebp-1c* were significantly elevated in individuals with MASLD, compared to normal livers (Figure 2A and B). Pearson correlation analysis further revealed that expression levels of *Nat10* and *Srebp-1c* were significantly and positively correlated (Figure 2C). Besides, correlation analysis suggested a significant and positive correlation between *Nat10* mRNA levels and hepatic TG contents (Figure 2D), as well as plasma TG and ALT levels (Figure 2E and F). Furthermore, expression levels of *Nat10* were also significantly correlated with the expression of inflammatory genes, including *Tnfa, Il1b* and *Il6* (Figure 2G—I). Taken together, our data indicate that hepatic *Nat10* is elevated in patients with MASLD and positively correlated with clinical characteristics.

3.4. Hepatocyte-specific NAT10 knockout mice are protected from HFD-induced liver steatosis

The abnormal expression of NAT10 in MASLD/MASH mice and patients with MASLD suggested that it may play a role in regulating hepatic lipid metabolism. Therefore, to examine the role of NAT10 *in vivo*, 8-week-old loxP-flanked NAT10 mice (NAT10 flox/flox) were fed a HFD diet for 10 weeks and then delivered with adenovirus containing Cre recombinase by tail-vein injection (Ad-Cre, Figure 3A). Adenovirus containing GFP was used as a negative control (Ad-GFP, Figure 3A). 2 weeks later, mice were sacrificed for subsequent analysis. A significant reduction in

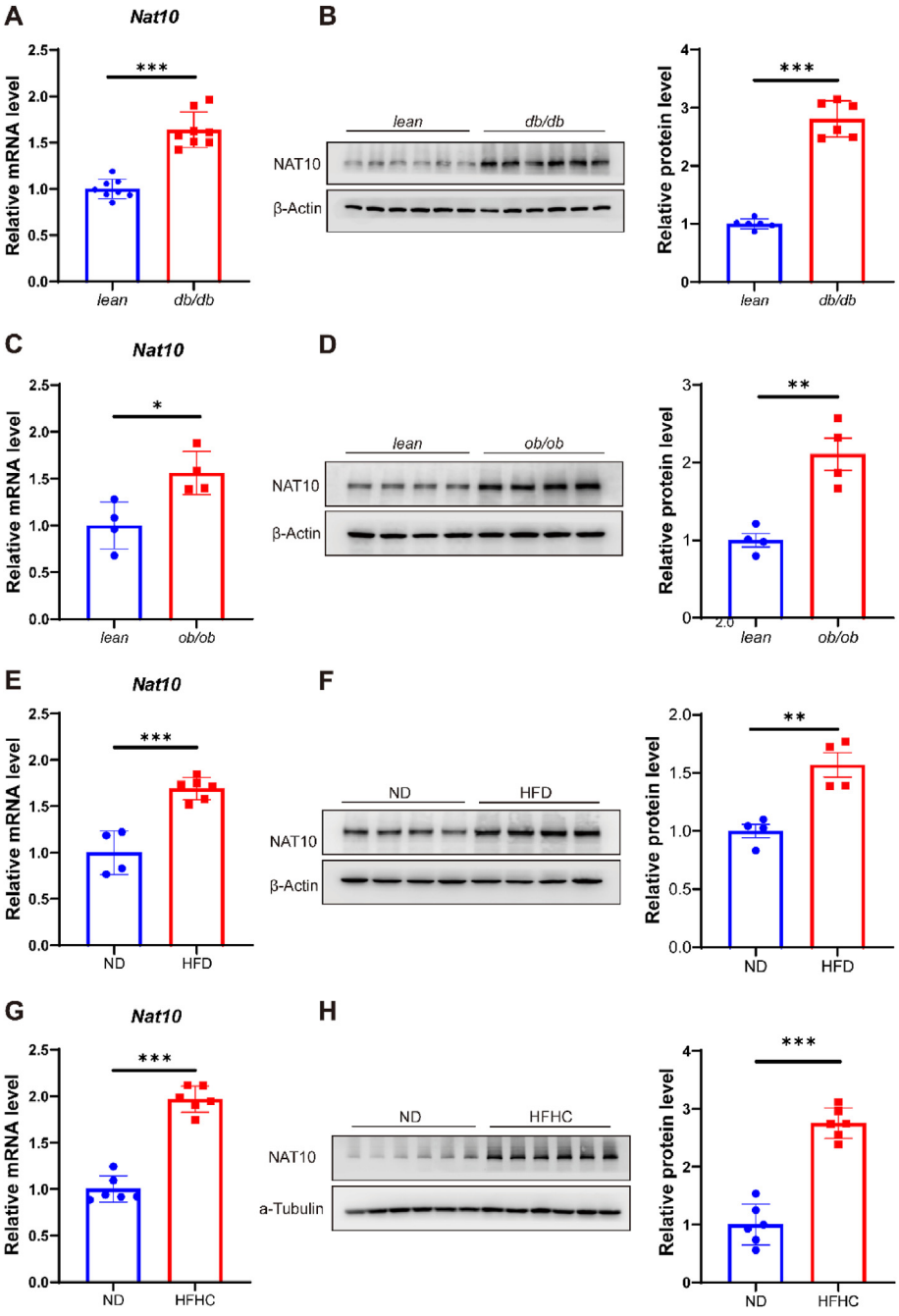

Figure 1: NAT10 expression is elevated in MASLD and MASH mice. (A, B) Relative mRNA expression and protein levels of NAT10 in the livers of *db/db* and *lean* mice. n = 8. (C—D) Relative mRNA expression and protein levels of NAT10 in the livers of *ob/ob* and *lean* mice. n = 4. (E—F) Relative mRNA expression and protein levels of NAT10 in the livers from HFD diet-induced MASLD mice or control mice. n = 4—6. (G—H) Relative mRNA expression and protein levels of NAT10 in the livers from HFHC diet-induced MASH mice or control mice. n = 6. All data were shown as the mean ± SEM. $^{*}P < 0.05$, $^{**}P < 0.01$, $^{***}P < 0.001$.

NAT10 expression levels was detected in the livers of mice injected with Ad-Cre compared to those injected with Ad-GFP (Figure 3B and C). In parallel, delivery of Ad-Cre did not affect NAT10 expression in skeletal muscle and white adipose tissues (Figure 3C). Although body weights, adipose tissues and food intake were not affected (Supplementary Figure 3A—F), liver weights and liver-to-body weight ratio were significantly reduced in the Ad-Cre injected mice (Figure 3D and E). Hepatic and plasma TG content was also reduced in mice with NAT10 deficiency (Figure 3F and G). Histology analysis also showed that HFD diet-induced hepatic steatosis was substantially attenuated in mice with NAT10 deficiency (Figure 3H).

To further determine the role of NAT10 mice in MASLD, NAT10 flox/flox mice were mated with Albumin-Cre mice to generate liver-specific NAT10 knockout mice, which will henceforth be referred to as NAT10 LKO (Figure 3I). Cre-negative NAT10 flox/flox littermates were employed as controls (hereinafter referred to as wild-type, WT). In the livers of LKO mice, NAT10 expression was reduced compared to WT mice (Figure 3J and K). WT and LKO mice were fed a HFD for 12

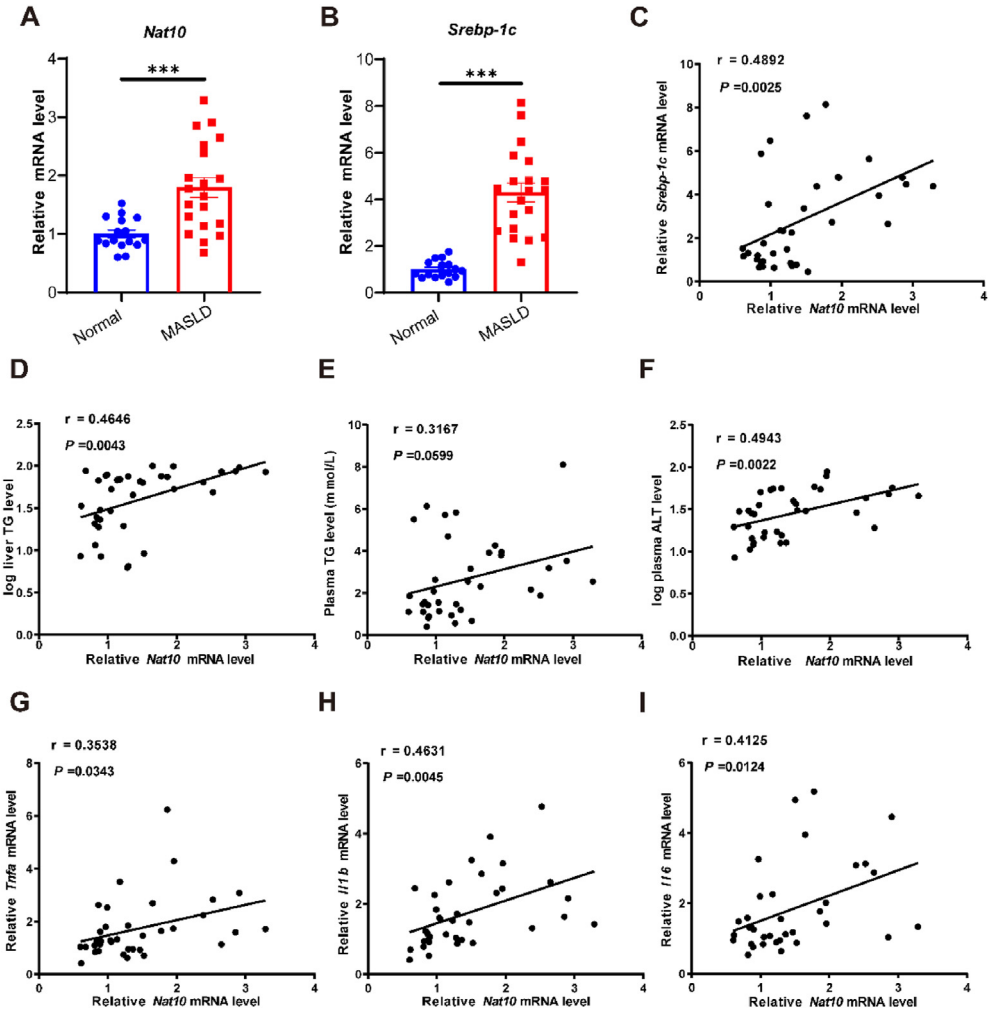

Figure 2: NAT10 expression is increased in patients with MASLD. (A, B) Relative mRNA levels of *Nat10*(A) and *Srebp-1c* (B) in normal livers (n = 16) and livers from patients with MASLD (n = 20). (C–I) Pearson *R* and *P* values for normalized *Nat10* mRNA levels versus *Srebp-1c* mRNA levels, liver TG contents, plasma TG contents plasma ALT contents, *Tnfa, Il1b*, and *Il6* mRNA levels in human livers (n = 36).

weeks. While body weights, adipose tissues and food intake were comparable (Supplementary Figure 3G–L), liver weights, liver-to-body weight ratio, and hepatic and plasma TG contents were significantly decreased in the LKO mice (Figure 3L–O). Histology analysis confirmed that lipid accumulation was reduced in the livers of NAT10 LKO mice (Figure 3P). Taken together, these results indicate that liver-specific suppression of NAT10 could protect mice from HFD-induced liver steatosis.

3.5. Hepatocyte-specific NAT10 knockout mice are protected from HFHC-induced MASH

We further tested the possible role of NAT10 in long-term HFHC diet-induced MASH. NAT10 flox/flox mice were fed a HFHC diet for 20 weeks and then administered with Ad-Cre or Ad-GFP to knockout NAT10 expression in the liver (Figure 4A and B). While body weights were comparable between two groups of mice (Figure 4C), liver weights and liver-to-body weight ratio were significantly reduced in the Ad-Cre injected mice (Figure 4D and E). Hepatic and plasma TG contents, and plasma total cholesterol levels were reduced in mice with NAT10 deficiency (Figure 4F–H). Plasma ALT and AST levels were also decreased, indicative of improved liver injury (Figure 4I and J). Hepatic TG accumulation in NAT10-deficient mice was also confirmed by hematoxylin and eosin (H&E) and Oil Red O staining (Figure 4K). Besides, F4/80, Masson, and Sirius red staining indicated that hepatic inflammation and fibrosis were significantly alleviated by NAT10 deficiency (Figure 4K–N). Hydroxyproline contents were reduced in the HFHC-fed mice administered with Ad-Cre, suggesting that NAT10 deficiency improved collagen deposition in the liver (Figure 4O). Besides, genes associated with hepatic inflammation, neutrophil infiltration, and fibrogenesis were reduced (Figure 4P and Q). Collectively, these results demonstrated that inhibition of NAT10 in the liver could improve MASH, suggesting that NAT10 plays an important pathogenic role in MASH progression.

3.6. NAT10 overexpression aggravated hepatic lipid deposition in mice under high-fat-diet condition

To complement the loss-of-function approach, two approaches were used to explore whether liver-specific overexpression of NAT10 can promote liver steatosis. C57BL/6 mice were administered with adenovirus (Ad-) carrying either NAT10 or GFP via tail vein injection. As shown in Supplementary Figure 4A–H, no significant differences were observed in body weight, liver weight, liver/body weight ratio, levels of

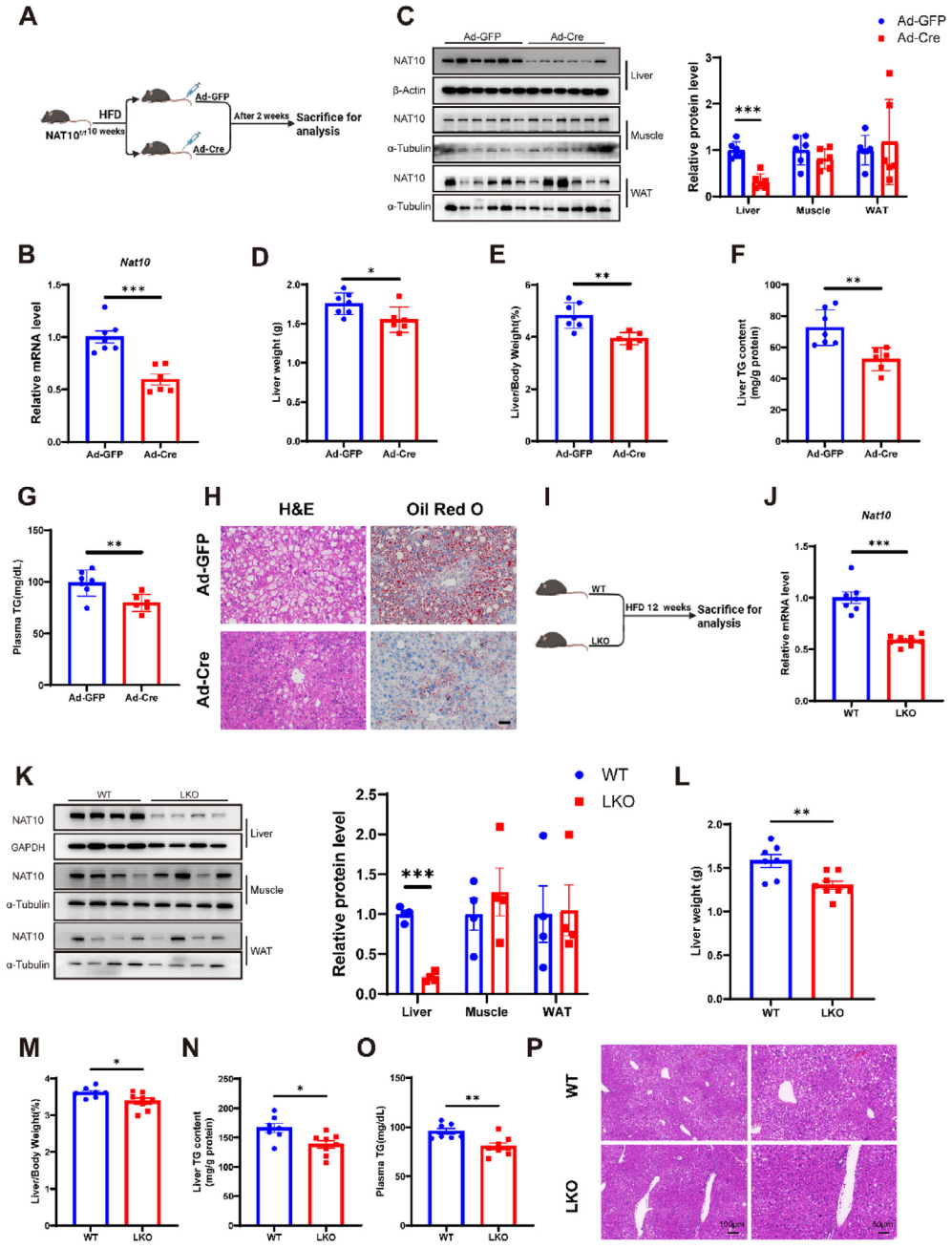

Figure 3: Hepatocyte-specific NAT10 knockout mice are protected from HFD-induced liver steatosis. (A) Experimental design. NAT10 flox/flox were fed a HFD diet for 10 weeks. Then, mice were injected with adenovirus targeting Cre or GFP control for 2 weeks. n = 6–7 per group. (B) Relative mRNA level of *Nat10* in the livers of NAT10 flox/flox mice administrated with Ad-Cre or Ad-GFP. (C) Protein levels of NAT10 in liver, muscle and WAT in two groups of mice. (D) Liver weights. (E) Liver/body weight ratio. (F) Liver TG content. (G) Plasma TG levels. (H) Liver histology analysis, including H&E and Oil Red O. Scale bar, 50 μm. (I) Experimental design. Liver-specific NAT10 knockout mice (LKO) were achieved by crossing Albumin-Cre mice with NAT10 flox/flox mice. n = 7–8 per group. (J) Relative mRNA level of *Nat10* in the livers of two groups of mice. (K) Protein levels of NAT10 in liver, muscle and WAT in two groups of mice. (L) Liver weights. (M) Liver/body weight ratio. (N) Liver TG content. (O) Plasma TG levels. (P) Liver histology analysis by H&E staining. Left: magnification: ×100, scale bar, 100 μm. Right: magnification: ×200, Scale bar, 50 μm. All data were shown as the mean ± SEM. $^{*}P < 0.05$, $^{**}P < 0.01$, $^{***}P < 0.001$.

liver TG, serum TG, total cholesterol and liver histopathology, between Ad-GFP and Ad-NAT10 mice under the normal chow diet. Then, C57BL/6 male mice were fed a HFD diet for 6 weeks and then administered with Ad-NAT10 or Ad-GFP. 2 weeks later, mice were sacrificed for analysis (Figure 5A). Protein levels of NAT10 were specifically elevated in the livers of mice administered with Ad-NAT10 compared with Ad-GFP groups (Figure 5B). Although body weights, adipose tissues and food intake were not affected (Supplementary Figure 5A–F), liver weights and liver-to-body weight ratio were significantly increased in mice with NAT10 overexpression (Figure 5C and D). Besides, hepatic and plasma TG contents and plasma ALT levels were elevated in Ad-NAT10-injected mice (Figure 5E–G). Histology analysis showed that Ad-NAT10-infected mice developed hepatic steatosis as depicted by H&E and Oil Red O staining (Figure 5H).

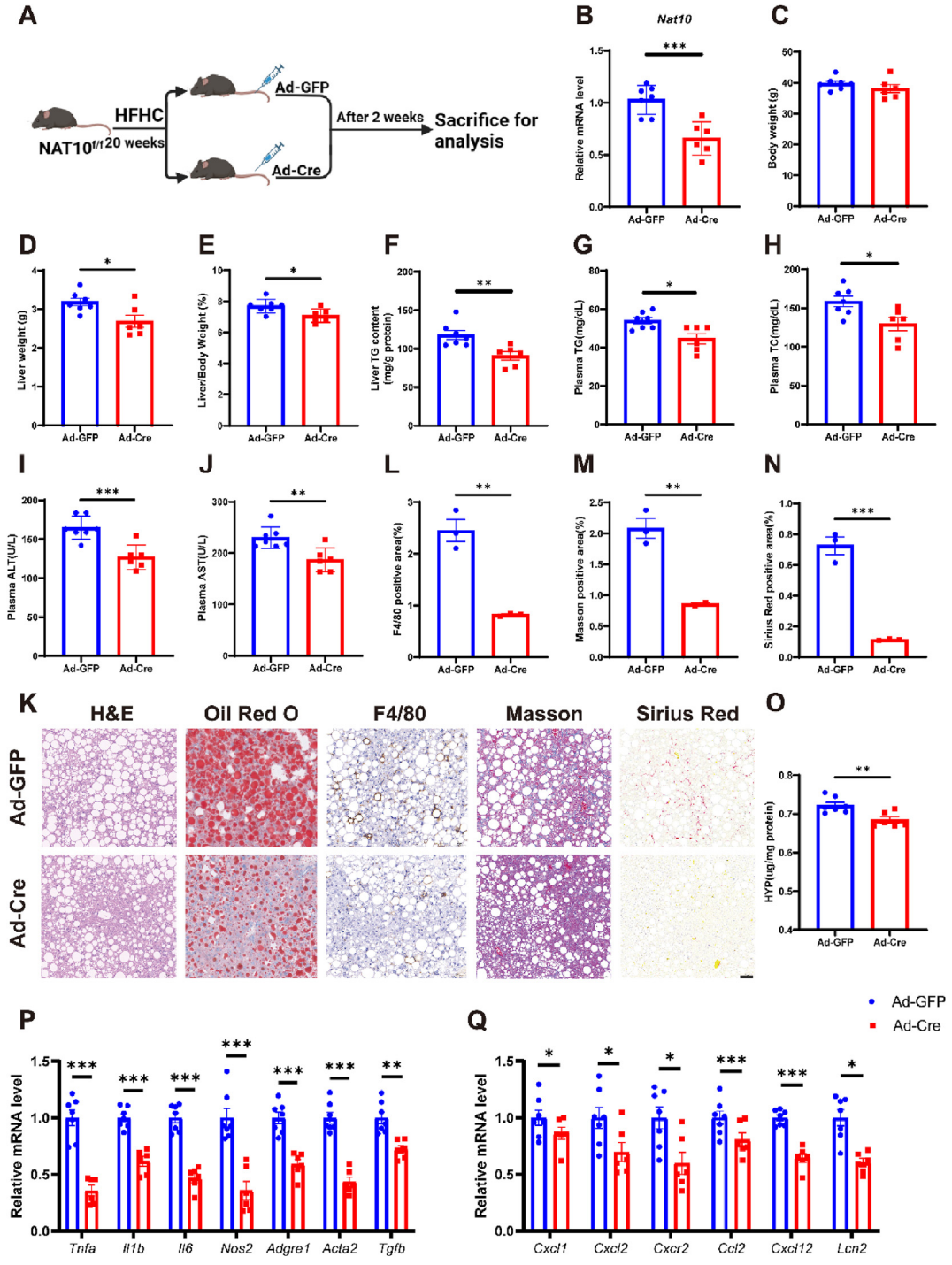

Figure 4: NAT10 knockout mice are protected from HFHC-induced MASH. (A) Experimental design. NAT10 flox/flox mice were fed a HFHC diet for 20 weeks and administered with adenovirus containing Cre or GFP control for 2 weeks. n = 6–7 per group. (B) Relative mRNA levels of *Nat10* in the livers of NAT10 flox/flox mice infected with Ad-Cre or Ad-GFP. (C) Body weights. (D) Liver weights. (E) Liver/body weight ratio. (F) Liver TG content. (G and H) Plasma TG total and cholesterol levels. (I and J) Plasma ALT and AST levels. (K) Liver histology and pathology analysis, including H&E, Oil Red O, F4/80, Masson staining and Sirius red. Scale bar, 50 μm. (L–N) Quantitation of F4/80, Masson staining and Sirius red. (O) Liver hydroxyproline contents. (P, Q) Relative mRNA levels of genes involved in liver inflammation and fibrosis (P) and neutrophil infiltration (Q). All data were showed as the mean ± SEM. $^{*}P < 0.05$, $^{**}P < 0.01$, $^{***}P < 0.001$.

On the other hand, adeno-associated virus (AAV)-mediated gene transduction was used. AAV-mediated gene expression is known to avoid immune response and can be expressed in liver for several months [27]. C57BL/6 mice were administered with AAV8 containing *Nat10* gene or GFP driven by a liver thyroid hormone-binding globulin promoter through tail-vein injection. Mice were kept on a HFD diet and sacrificed at 4 weeks post-injection (Figure 5I and J). Although body weights, adipose tissues and food intake were comparable (Supplementary Figure 5G–L), liver weights, liver-to-body weight ratio, hepatic and plasma TG contents, plasma ALT and lipid droplet

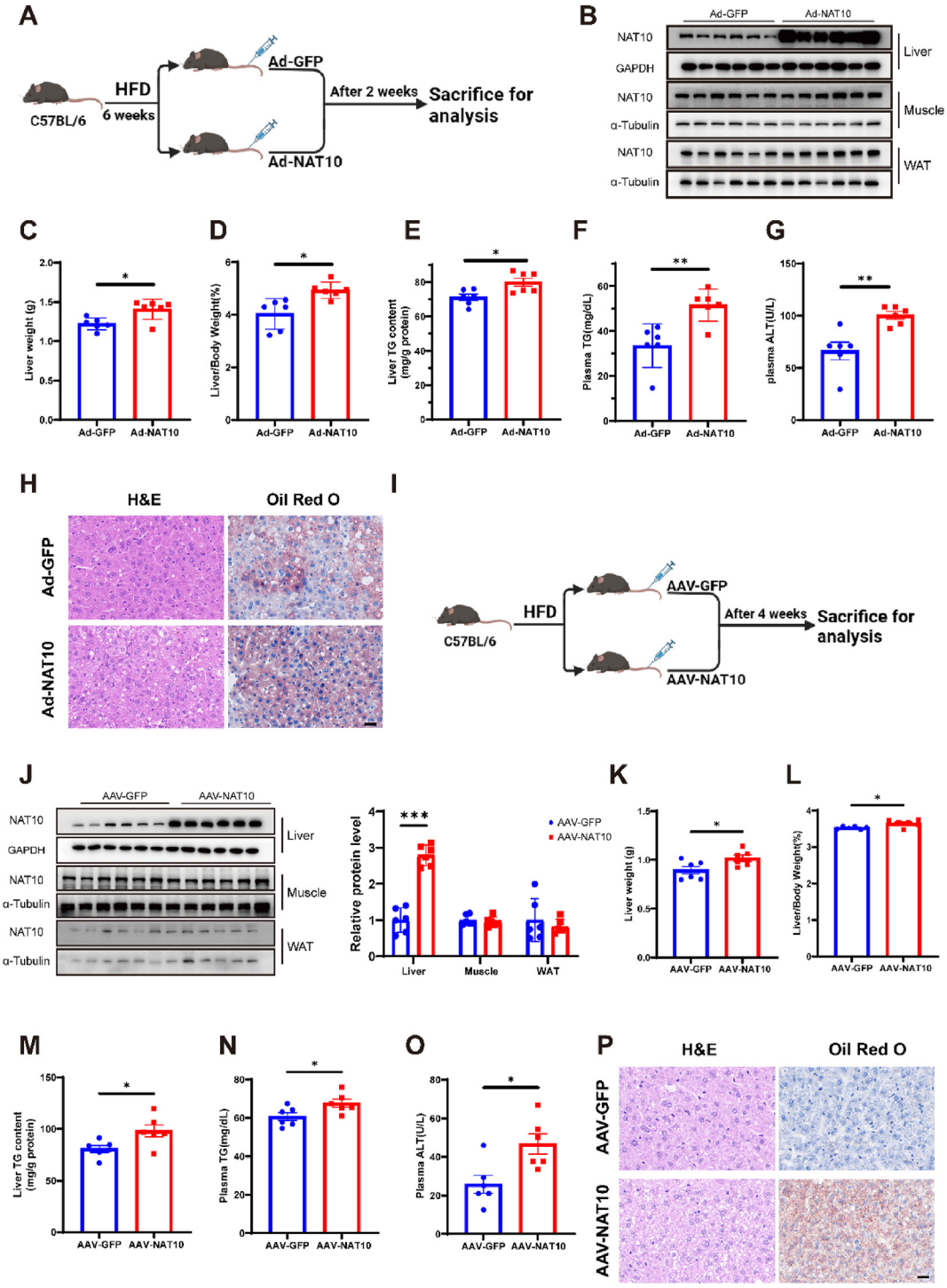

Figure 5: Liver-specific overexpression of NAT10 promotes hepatic lipid accumulation. (A) Experimental design. 8-week-old C57BL/6 male mice were fed a HFD diet for 6 weeks and administered with adenovirus targeting NAT10 or GFP control for 2 weeks. n = 6 per group. (B) Protein levels of NAT10 in the liver, muscle and WAT in C57BL/6 mice infected with Ad-NAT10 or Ad-GFP. (C) Liver weights. (D) Liver/body weight ratio. (E) Liver TG content. (F) Plasma TG levels. (G) Plasma ALT levels. (H) Liver histology analysis, including H&E and Oil Red O. Scale bar, 50 μm. (I) Experimental design. C57BL/6 mice were fed a HFD diet and injected with adeno-associated virus targeting NAT10 or GFP for 4 weeks. n = 6 per group. (J) Protein levels of NAT10 in the liver, muscle and WAT in C57BL/6 mice infected with AAV- NAT10 or AAV-GFP. (K) Liver weights. (L) Liver/body weight ratio. (M) Liver TG content. (N) Plasma TG level. (O) Plasma ALT levels. (P) Liver histology analysis, including H&E and Oil Red O. Scale bar, 50 μm. All data were shown as the mean ± SEM. $^{*}P < 0.05$, $^{**}P < 0.01$, $^{***}P < 0.001$.

accumulation in AAV-NAT10 mice were also significantly increased as compared to control mice (Figure 5K—P). Taken together, these data indicate that NAT10 overexpression could aggravate liver steatosis in mice under high-fat-diet condition.

3.7. NAT10 increased the expression and mRNA stability of *Srebp-1c*

We next determined the intrinsic mechanism by which NAT10 promotes liver steatosis. Our ac4C-Seq suggested that RNA acetylation is involved in the regulation of genes related to lipid biosynthesis (Supplementary Figure 1E). Besides, mRNA levels of *Nat10* and *Srebp-1c* are positively and significantly correlated in human livers (Figure 2C). To clarify the potential target(s) of NAT10, we conducted RIP-seq using liver samples from mice injected with AAV-NAT10 or AAV-GFP. A pronounced elevation in NAT10 binding transcripts was observed and mainly localized to the coding sequences (CDS) and 3′ -untranslated regions of genes (3′-UTR) (Supplementary Figure 6A and B). GO analysis further indicated that these NAT10-binding genes were involved in lipid metabolism pathways (Supplementary Figure 6C). Notably, the distribution of NAT10-binding regions of lipogenic genes, including *Srebf1, Fasn, Acc1*, and *Scd1*, was upregulated by NAT10 overexpression (Figure 6A and Supplementary Figure 6D—F). Consistently with the RIP-seq results, RNA immunoprecipitation using a NAT10 antibody resulted in an 18-fold enrichment of *Srebp-1c* mRNA. Similarly, ac4C RIP-qPCR detected a marked enrichment, suggesting a strong physical binding of NAT10 and ac4C with *Srebp-1c* mRNA (Figure 6B and C). Additionally, we observed a significant increase in the ac4C modification of the *Srebp-1c* gene in mouse primary hepatocytes overexpressing NAT10 (Figure 6D). Thus, all of these data suggest that NAT10 might regulate *Srebp-1c* mRNA modification and expression.

In agreement with our hypothesis, mRNA expression levels of *Srebp-1c* and its target genes, including *Fasn, Scd1* and *Acc1* were reduced in mice with NAT10 suppression (Figure 6E and G). Downregulation of SREBP-1c was further confirmed by western blots (Figure 6F and H). On the other hand, expression levels of *Srebp-1c*, *Fasn, Scd1* and *Acc1* were increased in the livers of mice expressing Ad-NAT10 or AAV-NAT10 (Figure 6I—L). These results indicate that *Srebp-1c* is a target of NAT10.

To further confirm the regulatory relationship between SREBP-1c and NAT10 *in vitro*, we isolated mouse primary hepatocytes (MPHs) from wild-type and liver-specific NAT10 knockout (LKO) mice. Cellular TG contents and expression levels of lipogenic genes were lower in MPHs from NAT10 LKO mice (Supplementary Figure 7A—C). In addition, MPHs from C57BL/6 mice were infected with adenovirus containing NAT10 or GFP. Accordingly, cellular TG contents and expression levels of lipogenic genes were increased in MPHs overexpressing NAT10 (Supplementary Figure 7D—F).

Besides, we detected a downregulation of genes involved in fatty acid β-oxidation (*Mcad, Acox1, Ppara, Cpt1a*) in the livers of NAT10 knockout mice (Supplementary Figure 8A and B). In agreement, lipid oxidation-related genes were upregulated in the livers of mice expressing Ad-NAT10 or AAV-NAT10 (Supplementary Figure 8C and D). Seahorse assays demonstrated that extracellular respiration (ECR) and fatty acid oxidation (FAO) were significantly reduced in the absence of NAT10 (Supplementary Figure 8E—H). We speculate that the reduction of fatty acid oxidation in the livers of NAT10-deficient mice might be attributed to the lower lipogenesis and lipid contents.

Afterwards, we examined the impacts of NAT10 on the mRNA lifetime of *Srebp-1c*. Hepa1-6 cells were transfected with Ad-NAT10 or Ad-GFP and harvested at different time points upon treatment with actinomycin D, an inhibitor of transcription. Overexpression of NAT10 led to an extended lifetime of *Srebp-1c* mRNA (Figure 6M). We also compared *Srebp-1c* mRNA lifetime in primary hepatocytes isolated from NAT10 WT and LKO mice. Compared with WT hepatocytes, *Srebp-1c* mRNA lifetime was reduced in hepatocytes from NAT10 LKO mice (Figure 6N). In conclusion, NAT10 could bind with *Srebp-1c* mRNA to catalyze acetylation modification, thereby increasing its mRNA stability and expression, which in turn upregulates lipogenic enzymes to promote MASLD and MASH.

To clarify if SREBP-1c is required for NAT10's effects, we used siRNA to knockdown SREBP-1c expression in MPHs. We found that knockdown of SREBP-1c largely attenuated the effects of NAT10 on increasing cellular TG contents (Figure 6O—Q). Thus, we speculate that NAT10's lipid synthetic effects were, at least in part, dependent on SREBP-1c. In conclusion, our results demonstrated that NAT10 could bind with *Srebp-1c* mRNA to catalyze acetylation modification, thereby increasing its mRNA stability and expression, which in turn upregulates lipogenic enzymes to promote MASLD and MASH.

3.8. Therapeutic effects of suppressing NAT10 in treating MASLD in mice

Based on the results from genetic inactivation and overexpression, we speculate that pharmacologic suppression of NAT10 may provide a novel strategy to treat MASLD. Remodelin was used as an inhibitor of NAT10 to perform *in vivo* experiments in several newly studies [18,28]. Thus, C57BL/6 mice were fed on a HFD for 8 weeks to induce MASLD and then treated with daily intraperitoneal injection of Remodelin or vehicle control for another 16 days (Figure 7A). The dosage of 20 mg/kg was used according to a recent study, which was also performed in a mouse model [18]. Interestingly, Remodelin treatment gradually reduced body weight in HFD mice (Figure 7B and C), which might be attributed to smaller adipose depots in brown adipose tissues and epididymal white adipose tissue (Supplementary Figure 9A—D). Besides, Remodelin significantly reduced liver weights (Figure 7D), liver TG contents, plasma TG and TC levels (Figure 7E—G). Macroscopic appearance and histology analysis of liver sections by H&E staining confirmed that hepatic steatosis was substantially improved in Remodelin-treated HFD mice (Figure 7H). In the group treated with Remodelin, there was a marked decrease in inflammatory cell infiltration, as demonstrated by F4/80 and Ly6g staining. In parallel, a reduction in collagen deposition was observed, evidenced by Masson's trichrome and Sirius Red staining. Inflammatory cell infiltration was reduced as shown by F4/80 and Ly6g staining (Supplementary Figure 9E). Besides, collagen deposition, as shown by Masson and Sirius Red staining, was also reduced by Remodelin (Supplementary Figure 9E). At the molecular level, Remodelin reduced expression levels of *Srebp-1c* and lipogenic enzymes (Figure 7I and J). Furthermore, mRNA levels of genes associated with liver inflammation and fibrosis were reduced in mice treated with Remodelin (Supplementary Figure 9F). These results indicate that pharmacological suppression of NAT10 could ameliorate MASLD and related pathologies in mice.

4. DISCUSSION

NAT10-mediated ac4C was identified as a novel RNA modification to regulate translation efficiency and stability of mRNAs [17,29,30]. However, its pathogenic roles in human diseases remain largely unexplored. In the present study, we found that NAT10, an ac4C catalytic enzyme reader, was upregulated in the livers of multiple mouse models of MASLD and MASH. Furthermore, we identified NAT10 as a novel regulator of hepatic steatosis through catalysis of ac4C modification and promoting the mRNA stability of *Srebp-1c*. This is supported

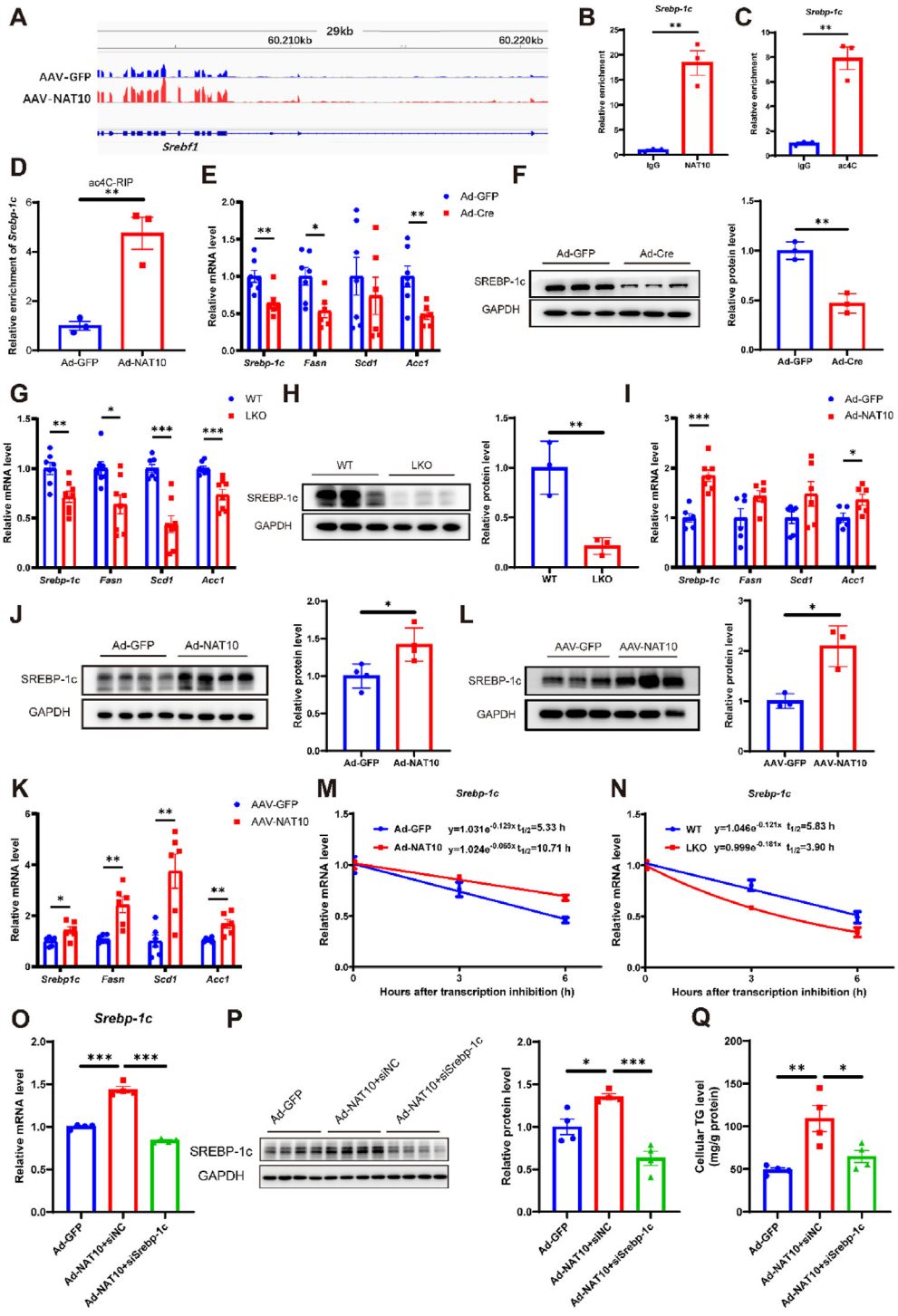

Figure 6: NAT10 increases the expression and mRNA stability of *Srebp-1c*. (A) Integrative Genomics Viewer (IGV) tracks displaying the NAT10 binding region of *Srebf1* from RIP-seq. (B) Enrichment showing the binding of NAT10 on the mRNA of *Srebp-1c* in Hepa1-6 cells determined by RNA immunoprecipitation (RIP). IgG was used as a negative control. n = 3. (C) RIP assays showing the binding of ac4C on the mRNA of *Srebp-1c* in Hepa1-6 cells. IgG was used as a negative control. n = 3. (D) The enrichment of the binding of ac4C on the mRNA of *Srebp-1c*. Mouse primary hepatocytes were infected with Ad-GFP or Ad-NAT10 and subjected to RNA immunoprecipitation (RIP) assays. n = 3. (E and F) Relative mRNA levels of lipid synthesis genes and protein levels of SREBP-1c in the livers of NAT10 flox/flox mice infected with Ad-Cre or Ad GFP. (G and H) Relative mRNA levels of lipid synthesis genes and protein levels of SREBP-1c in the livers of NAT10-WT and NAT10-LKO mice. (I and J) Relative mRNA levels of lipid synthesis genes and protein levels of SREBP-1c in the livers of C57BL/6 mice infected with Ad-NAT10 or Ad-GFP. (K and L) Relative mRNA levels of lipid synthesis genes and protein levels of SREBP-1c in the livers of C57BL/6 mice infected with AAV- NAT10 or AAV-GFP. (M) Decay of *Srebp-1c* mRNA in Hepa1-6 cells with NAT10 overexpression versus control. (N) Decay of *Srebp-1c* mRNA decline in mouse primary hepatocytes from NAT10-LKO or NAT10-WT mice. (O and P) Relative mRNA levels of lipogenic genes, and protein levels of SREBP-1c in MPHs. (Q) Cellular TG levels in MPHs transfected with Ad-GFP plus negative control siRNA (siNC), Ad-NAT10 plus siNC, or Ad-NAT10 plus siRNA targeting Srebp-1c (siSrebp-1c). All data were shown as the mean ± SEM. $*P < 0.05$, $**P < 0.01$, $***P < 0.001$.

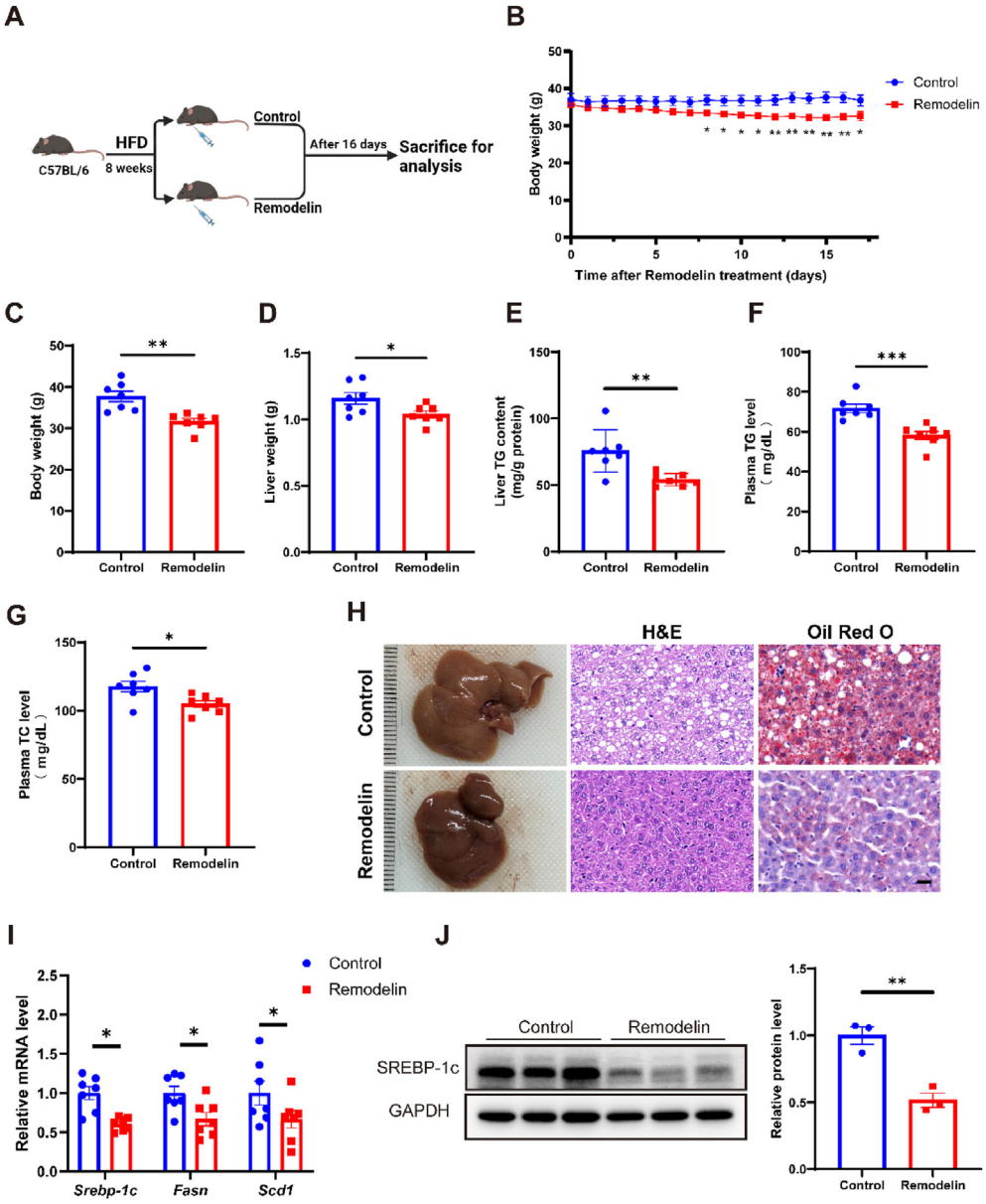

Figure 7: Remodelin improves liver steatosis in preclinical mouse model. (A–J) C57BL/6 mice were fed on a HFD for 8 weeks and then treated with daily intraperitoneal injection of Remodelin or vehicle control (Control) for another 16 days. n = 7. (A) Experimental design of two groups of mice. (B) Body weight curve during treatment. (C) Body weight at the experimental endpoint. (D) Liver weight. (E) Liver TG contents. (F and G) Plasma TG and TC levels. (H) Representative macroscopic appearance and histology analysis by H&E and Oil Red O staining. Scale bar, 50 μm. (I) Relative mRNA levels of lipid synthesis genes in the livers. (J) Protein levels of SREBP-1c in the livers. All data were shown as the mean ± SEM. $^{*}P < 0.05$, $^{**}P < 0.01$, $^{***}P < 0.01$.

by multiple lines of evidence. First, hepatic NAT10 is upregulated in multiple MASLD and MASH mice models. NAT10 expression is also elevated in the livers of patients with MASLD and significantly correlated with clinical characteristics. Second, hepatic NAT10 deficiency reduced TG accumulation in the livers of MASLD mice, while its overexpression significantly exacerbated HFD-induced liver steatosis. NAT10 deficiency improved TG retention-related liver inflammation, injury and fibrosis in MASH mice. Third, NAT10 could catalyze ac4C modification of *Srebp-1c* mRNA to increase its stability and expression. Consequently, NAT10 increases the mRNA and protein levels of SERBP-1c, thus upregulating lipogenic enzymes to promote liver steatosis. Therefore, our findings identify a NAT10-dependent pathway that promotes MASLD and MASH.

NAT10 is a member of the Gcn5-related N-acetyltransferase (GNAT) family and contains 1025 amino acids with a molecular weight of 116 kDa [31]. There are three conserved structural domains in the NAT10 protein: the N-terminal acetylase structural domain, the ATP/guanosine triphosphate (GTP) binding motif, and the ATPase structural domain [17,32]. NAT10 functions as a writer for ac4C, regulating the expression of ac4C-modified target genes through translation or RNA stability [33–36]. Recent studies have shown that NAT10 is upregulated in several types of tumors and its expression is correlated with the expansion and proliferation of cancer cells. For example, NAT10/ac4C/FOXP1 regulatory axis promotes malignant progression and facilitates immunosuppression by reprogramming glycolytic metabolism in cervical cancer [37]. Besides, lysine 2-hydroxyisobutyrylation and

enhanced protein stability of NAT10 in esophageal squamous cell carcinoma promotes cancer metastasis in an ac4C-dependent manner [38]. N4-Acetylcytidine drives glycolysis addiction in gastric cancer via NAT10/SEPT9/HIF-1alpha positive feedback loop [39]. These studies highlighted the dynamic and reversible ac4C modification on specific mRNAs as a potential intervention for cancer. In this study, we focused on the association of ac4C modification with MASLD pathogenesis by profiling the ac4C landscape in the livers of *db/db* and *lean* mice. Subsequent combined analysis of acRIP-Seq and RNA-Seq revealed simultaneous elevation of ac4C modification and mRNA levels in genes involved in lipid metabolism and lipogenesis in *db/db* mice, indicating a strong relationship between the altered ac4C acetylation and increased lipogenic genes expression.

The translational significance of our study is that treatment of Remodelin, an NAT10 inhibitor, could improve liver steatosis and dyslipidemia in a mouse model of MASLD, although intensive studies are still warranted to fully assess the therapeutic effects and safety in larger animals. Besides, we noticed that Remodelin treatment could gradually reduce body weights and adipocyte size in obese mice (Figure 7B and Supplementary Figure 9 A—D), suggesting that systemic administration of Remodelin may induce metabolic changes in other tissues like BAT and eWAT. Therefore, whether suppression of NAT10 in BAT and eWAT is responsible for the reduced body weights deserves further research. Collectively, our findings using a preclinical mouse model demonstrate the therapeutic potential of Remodelin in improving MASLD. We propose that hepatocyte-specific delivery of NAT10 inhibitor or siRNA/shRNA may provide more effective strategies for treatment MASLD.

Several limitations in our study should be pointed out. First, we could not exclude the possibility that NAT10 may regulate hepatic lipid metabolism by other mechanisms, in addition to increasing SREBP-1c expression. RNA pull down might help to explore more downstream target genes for NAT10 in the liver. Additionally, NAT10 may also regulate the redistribution of lipids within the liver. Spatial transcriptomics would be required to explore this issue. Second, NAT10 has been shown to regulate the inflammatory process in neutrophils [40], which is an important component in the development of chronic liver diseases [41,42]. Thus, the molecular mechanism by which NAT10 regulates the inflammatory response and collagen deposition in MASH requires future work. Finally, our study demonstrated that Remodelin could ameliorate liver steatosis and inflammation in HFD-induced MASLD mice. However, none of diets can perfectly mimic the pathogenesis of human MASH [43]. Thus, the therapeutic effects of Remodelin on MASH should be further examined by additional models, such as GAN diet- and CD-HFD-induced MASH.

In summary, our gain- and loss-of-function studies demonstrate that NAT10 plays a critical role in liver steatosis and the development of MASLD and MASH through ac4C modification of *Srebp-1c* mRNA. Together, this work provided evidence that suppressing the expression or function of NAT10 may provide a new therapeutic approach for treating MASLD and MASH.

CREDIT AUTHORSHIP CONTRIBUTION STATEMENT

Yanying Yang: Formal analysis, Data curation, Conceptualization. **Jie Lu:** Visualization, Validation. **Yuejun Liu:** Investigation, Conceptualization. **Ni Zhang:** Supervision, Software. **Yunchen Luo:** Validation, Supervision. **Mingyue Ma:** Methodology, Investigation. **Zhixia Dong:** Methodology, Software. **Shuo Zhang:** Investigation. **Ming-Hua Zheng:** Visualization, Validation. **Cheng-Chao Ruan:** Investigation, Formal analysis. **Xinjian Wan:** Formal analysis. **Cheng Hu:** Visualization, Supervision. **Yan Lu:** Investigation, Funding acquisition. **Xiaojing Ma:** Validation, Supervision. **Bing Zhou:** Supervision, Resources, Project administration.

ACKNOWLEDGMENTS

This study was supported by the National Natural Science Foundation of China (82300966 to B.Z. and 82270918 to Y. Liu), the Young Elite Scientists Sponsorship Program by China Association for Science and Technology (2023QNRC001 to B.Z.), Shanghai Sailing Program by Shanghai Municipal Science and Technology Committee (22YF1432800 to B.Z.) and China Postdoctoral Science Foundation Funded Project (2021M702183 to B.Z.)

DECLARATION OF COMPETING INTEREST

No potential conflicts of interest relevant to this article were reported.

DATA AVAILABILITY

All acRIP-seq and RIPseq -data generated in this work have been deposited into the Gene Expression Omnibus (GEO) database (GSE275575, GSE275576). Other data will be made available on request.

APPENDIX A. SUPPLEMENTARY DATA

Supplementary data to this article can be found online at https://doi.org/10.1016/j.molmet.2024.102030.

REFERENCES

[1] Feng G, Valenti L, Wong VW, Fouad YM, Yilmaz Y, Kim W, et al. Recompensation in cirrhosis: unravelling the evolving natural history of nonalcoholic fatty liver disease. Nat Rev Gastroenterol Hepatol 2024;21:46—56.
[2] Hsu CL, Loomba R. From NAFLD to MASLD: implications of the new nomenclature for preclinical and clinical research. Nat Metab 2024;6(4):600—2.
[3] Huang DQ, Singal AG, Kono Y, Tan DJH, El-Serag HB, Loomba R. Changing global epidemiology of liver cancer from 2010 to 2019: NASH is the fastest growing cause of liver cancer. Cell Metab 2022;34:969—977.e2.
[4] Tan DJH, Setiawan VW, Ng CH, Lim WH, Muthiah MD, Tan EX, et al. Global burden of liver cancer in males and females: changing etiological basis and the growing contribution of NASH. Hepatology 2023;77:1150—63.
[5] Lonardo A, Mantovani A, Petta S, Carraro A, Byrne CD, Targher G. Metabolic mechanisms for and treatment of NAFLD or NASH occurring after liver transplantation. Nat Rev Endocrinol 2022;18:638—50.
[6] Batchuluun B, Pinkosky SL, Steinberg GR. Lipogenesis inhibitors: therapeutic opportunities and challenges. Nat Rev Drug Discov 2022;21:283—305.
[7] Hendrix S, Kingma J, Ottenhoff R, Valiloo M, Svecla M, Zijlstra LF, et al. Hepatic SREBP signaling requires SPRING to govern systemic lipid metabolism in mice and humans. Nat Commun 2023;14:5181.
[8] Guan D, Bae H, Zhou D, Chen Y, Jiang C, La CM, et al. Hepatocyte SREBP signaling mediates clock communication within the liver. J Clin Investig 2023;133.
[9] Gosis BS, Wada S, Thorsheim C, Li K, Jung S, Rhoades JH, et al. Inhibition of nonalcoholic fatty liver disease in mice by selective inhibition of mTORC1. Science 2022;376:eabf8271.
[10] Jeon YG, Kim YY, Lee G, Kim JB. Physiological and pathological roles of lipogenesis. Nat Metab 2023;5:735—59.
[11] Jeon TI, Osborne TF. SREBPs: metabolic integrators in physiology and metabolism. Trends Endocrinol Metab 2012;23:65—72.

[12] Jiao Y, Zhao J, Zhang Z, Li M, Yu X, Yang Y, et al. SRY-box containing gene 4 promotes liver steatosis by upregulation of SREBP-1c. Diabetes 2018;67:2227–38.
[13] Lu Y, Ma Z, Zhang Z, Xiong X, Wang X, Zhang H, et al. Yin Yang 1 promotes hepatic steatosis through repression of farnesoid X receptor in obese mice. Gut 2014;63:170–8.
[14] Liu C, Zhou B, Meng M, Zhao W, Wang D, Yuan Y, et al. FOXA3 induction under endoplasmic reticulum stress contributes to non-alcoholic fatty liver disease. J Hepatol 2021;75:150–62.
[15] Guo Y, Zhang X, Zhao Z, Lu H, Ke B, Ye X, et al. NF- κ B/HDAC1/SREBP1c pathway mediates the inflammation signal in progression of hepatic steatosis. Acta Pharm Sin B 2020;10:825–36.
[16] Zhou B, Liu C, Xu L, Yuan Y, Zhao J, Zhao W, et al. N(6)-methyladenosine reader protein YT521-B homology domain-containing 2 suppresses liver steatosis by regulation of mRNA stability of lipogenic genes. Hepatology 2021;73:91–103.
[17] Arango D, Sturgill D, Alhusaini N, Dillman AA, Sweet TJ, Hanson G, et al. Acetylation of cytidine in mRNA promotes translation efficiency. Cell 2018;175:1872–1886 e24.
[18] Shi J, Yang C, Zhang J, Zhao K, Li P, Kong C, et al. NAT10 is involved in cardiac remodeling through ac4C-mediated transcriptomic regulation. Circ Res 2023;133:989–1002.
[19] Wang K, Zhou LY, Liu F, Lin L, Ju J, Tian PC, et al. PIWI-interacting RNA HAAPIR regulates cardiomyocyte death after myocardial infarction by promoting NAT10-mediated ac(4) C acetylation of Tfec mRNA. Adv Sci 2022;9:e2106058.
[20] Zhang Y, Jing Y, Wang Y, Tang J, Zhu X, Jin WL, et al. NAT10 promotes gastric cancer metastasis via N4-acetylated COL5A1. Signal Transduct Target Ther 2021;6:173.
[21] Fang T, Wang H, Pan X, Little PJ, Xu S, Weng J. Mouse models of nonalcoholic fatty liver disease (NAFLD): pathomechanisms and pharmacotherapies. Int J Biol Sci 2022;18:5681–97.
[22] Van Herck MA, Vonghia L, Francque SM. Animal models of nonalcoholic fatty liver disease – a starter's guide. Nutrients 2017;9.
[23] Friedman SL, Neuschwander-Tetri BA, Rinella M, Sanyal AJ. Mechanisms of NAFLD development and therapeutic strategies. Nat Med 2018;24:908–22.
[24] Gallage S, Avila JEB, Ramadori P, Focaccia E, Rahbari M, Ali A, et al. A researcher's guide to preclinical mouse NASH models. Nat Metab 2022;4:1632–49.
[25] Zhou B, Luo Y, Ji N, Hu C, Lu Y. Orosomucoid 2 maintains hepatic lipid homeostasis through suppression of de novo lipogenesis. Nat Metab 2022;4:1185–201.
[26] Xiang L, Li X, Luo Y, Zhou B, Liu Y, Li Y, et al. A multi-omic landscape of steatosis-to-NASH progression. Life Metab 2022;1:242–57.
[27] Samulski RJ, Muzyczka N. AAV-mediated gene therapy for research and therapeutic purposes. Annu Rev Virol 2014;1:427–51.
[28] Qu Z, Pang X, Mei Z, Li Y, Zhang Y, Huang C, et al. The positive feedback loop of the NAT10/Mybbp1a/p53 axis promotes cardiomyocyte ferroptosis to exacerbate cardiac I/R injury. Redox Biol 2024;72:103145.
[29] Dalhat MH, Narayan S, Serio H, Arango D. Dissecting the oncogenic properties of essential RNA-modifying enzymes: a focus on NAT10. Oncogene 2024;43:1077–86.
[30] Zhang Y, Lei Y, Dong Y, Chen S, Sun S, Zhou F, et al. Emerging roles of RNA ac4C modification and NAT10 in mammalian development and human diseases. Pharmacol Ther 2024;253:108576.
[31] Liu R, Wubulikasimu Z, Cai R, Meng F, Cui Q, Zhou Y, et al. NAT10-mediated N4-acetylcytidine mRNA modification regulates self-renewal in human embryonic stem cells. Nucleic Acids Res 2023;51:8514–31.
[32] Zheng J, Tan Y, Liu X, Zhang C, Su K, Jiang Y, et al. NAT10 regulates mitotic cell fate by acetylating Eg5 to control bipolar spindle assembly and chromosome segregation. Cell Death Differ 2022;29:846–60.
[33] Wang G, Zhang M, Zhang Y, Xie Y, Zou J, Zhong J, et al. NAT10-mediated mRNA N4-acetylcytidine modification promotes bladder cancer progression. Clin Transl Med 2022;12:e738.
[34] Yan Q, Zhou J, Wang Z, Ding X, Ma X, Li W, et al. NAT10-dependent N(4)-acetylcytidine modification mediates PAN RNA stability, KSHV reactivation, and IFI16-related inflammasome activation. Nat Commun 2023;14:6327.
[35] Deng M, Zhang L, Zheng W, Chen J, Du N, Li M, et al. Helicobacter pylori-induced NAT10 stabilizes MDM2 mRNA via RNA acetylation to facilitate gastric cancer progression. J Exp Clin Cancer Res 2023;42:9.
[36] Shenshen W, Yin L, Han K, Jiang B, Meng Q, Aschner M, et al. NAT10 accelerates pulmonary fibrosis through N4-acetylated TGFB1-initiated epithelial-to-mesenchymal transition upon ambient fine particulate matter exposure. Environ Pollut 2023;322:121149.
[37] Chen X, Hao Y, Liu Y, Zhong S, You Y, Ao K, et al. NAT10/ac4C/FOXP1 promotes malignant progression and facilitates immunosuppression by reprogramming glycolytic metabolism in cervical cancer. Adv Sci 2023;10:e2302705.
[38] Liao L, He Y, Li SJ, Yu XM, Liu ZC, Liang YY, et al. Lysine 2-hydroxyisobutyrylation of NAT10 promotes cancer metastasis in an ac4C-dependent manner. Cell Res 2023;33:355–71.
[39] Mei Z, Shen Z, Pu J, Liu Q, Liu G, He X, et al. NAT10 mediated ac4C acetylation driven m(6)A modification via involvement of YTHDC1-LDHA/PFKM regulates glycolysis and promotes osteosarcoma. Cell Commun Signal 2024;22:51.
[40] Zhang H, Chen Z, Zhou J, Gu J, Wu H, Jiang Y, et al. NAT10 regulates neutrophil pyroptosis in sepsis via acetylating ULK1 RNA and activating STING pathway. Commun Biol 2022;5:916.
[41] Hwang S, Yun H, Moon S, Cho YE, Gao B. Role of neutrophils in the pathogenesis of nonalcoholic steatohepatitis. Front Endocrinol 2021;12:751802.
[42] He Y, Rodrigues RM, Wang X, Seo W, Ma J, Hwang S, et al. Neutrophil-to-hepatocyte communication via LDLR-dependent miR-223-enriched extracellular vesicle transfer ameliorates nonalcoholic steatohepatitis. J Clin Investig 2021:131.
[43] Vacca M, Kamzolas I, Harder LM, Oakley F, Trautwein C, Hatting M, et al. An unbiased ranking of murine dietary models based on their proximity to human metabolic dysfunction-associated steatotic liver disease (MASLD). Nat Metab 2024;6(6):1178–96.

